A Simulation Study of Sperm Motility Hydrodynamics Near Fish Eggs and Spheres

Kenta Ishimoto[1,2*], Jacky Cosson[3†], Eamonn A. Gaffney[4‡].

[1] The Hakubi Center for Advanced Research, Kyoto University, Kyoto, 606-8501, Japan.

[2] Research Institute for Mathematical Sciences, Kyoto University, Kyoto, 606-8502, Japan.

[3] University of South Bohemia in Ceske Budejovice, Faculty of Fisheries and Protection of Waters, South Bohemian Research Center of Aquaculture and Biodiversity of Hydrocenoses, Research Institute of Fish Culture and Hydrobiology, Czech Republic

[4] Wolfson Centre for Mathematical Biology, Mathematical Institute, University of Oxford, Oxford OX2 6GG, UK.

[*] Author for correspondence.

Abstract

For teleost fish fertilisation, sperm must proceed through a small opening on the egg surface, referred to as the micropyle. In this paper, we have used boundary element simulations to explore whether the hydrodynamic attraction between sperm and a fish egg can be a sperm guidance cue. Hydrodynamical egg-sperm interactions alone do not increase the chances of an egg encounter, nor do they induce surface swimming for virtual turbot fish sperm across smooth spheres with a diameter of 1mm, which is representative of a turbot fish egg. When a repulsive surface force between the virtual turbot sperm and the egg is introduced, as motivated by surface charge and van-der-Waals interactions for instance, we find that extended surface swimming of the virtual sperm across a model turbot egg occurs, but ultimately the sperm escapes from the egg. This is due to the small exit angle of the scattering associated with the initial sperm-egg interaction at the egg surface, leading to a weak drift away from the egg, in combination with a weak hydrodynamical attraction between both gametes, though the latter is not sufficient to prevent eventual escape. The resulting transience is not observed experimentally but is a detailed quantitative difference between theory and observation in that stable surface swimming is predicted for eggs with radii larger than about 1.8mm. Regardless, the extended sperm swimming trajectory across the egg constitutes a two-dimensional search for the micropyle and thus the egg is consistently predicted to provide a guidance cue for sperm once they are sufficiently close. In addition, the observation that the virtual turbot sperm swims stably next to a flat plane given repulsive surface interactions, but does not swim stably adjacent to a turbot-sized egg, which is extremely large by sperm-lengthscales, also highlights that the stability of sperm swimming near a boundary is very sensitive to geometry.

Keywords: sperm motility, sperm guidance, low Reynolds number flow, fish egg, external fertilization

[*] ishimoto@kurims.kyoto-u.ac.jp

[†] jacosson@gmail.com

[‡] gaffney@maths.ox.ac.uk

1 Introduction

Flagellated spermatozoa are ubiquitous but ultra-specialised, with the function of propagating a genetic payload toward an egg for fertilization, driven by an active axoneme which induces cell motility via the action of dynein molecular motors, resulting in undulating flagellar oscillations [36]. Such a relatively uncluttered relationship between mechanics and biological function is rare and interests not only biologists, but also physicists, hydrodynamicists and applied mathematicians, who study the fluid and filament dynamics associated with sperm propulsion [35, 16, 19].

A breakthrough in the hydrodynamical understanding of sperm motility mechanics arose from the development of resistive force theory due to the joint work of a biologist and a hydrodynamicist, Gray and Hancock [22]. Whilst resistive force theory is simple to implement, it is relatively inaccurate and hence slender-body theory was developed in the 1970s and 1980s for mechanical studies of cellular swimming (e.g. [23, 31]). Nonetheless the additional complexity of slender-body theory, and the fact resistive force theory is reasonably accurate, at least for small cell bodies and away from surfaces [32], has entailed that resistive force theory has remained popular in numerous inter-disciplinary studies of cell swimming, for instance the works of Hines, Blum, Katz and Rikmenspoel among others [24, 25, 33, 41]. More recently, there has been a tremendous resurgence of theoretical interest in the field, predominantly driven by advances in computational speed and memory allowing sophisticated simulation studies, extending accuracy beyond slender body theories, for example via the use of boundary elements [21, 27], as required for studying the subtle dynamics of boundary accumulation [27]. In addition, numerical approaches are now regularly coupled with the digital revolution of video-microscopy, with the latter providing extensive quantitative spatio-temporal data for cell motility studies [40, 47, 18].

However, with the prime exception of sea urchin sperm, which are often described as the *E. coli* of fertilisers, externally fertilising sperm have been neglected in these interdisciplinary studies. This neglect is despite the fact fish spermatology is a mature field supporting the needs of aquaculture sperm-banking and biotechnology [52]. In particular, to improve our understanding of how and why fish sperm cells behave and to improve the characterisation, classification and understanding of reconstituted sperm from cryo-preserved stocks, aquatic reproductive physiology laboratories have exploited the digital revolution of video-microscopy, providing extensive data (see Fig. 1a for example). Furthermore, fish sperm often exhibit behaviour not seen in mammals, such a limited duration of beating, which can be less than a minute after activation [10].

In particular, the limited beat duration is exhibited by our exemplar of turbot sperm below: the initial flagellar waveform is illustrated in Fig 1a and persists for approximately 30 seconds after activation via contact with higher osmolarity solutions [7], such as seawater. During this early-stage of active beating, turbot sperm swim at speeds of approximately 150-200 μm/s [7, 12], after which the flagellar waveform transitions relatively abruptly to one which is distally subdued and with a slightly shorter wavelength. This late-stage of flagellar beating is illustrated by Fig 1b, which presents the waveform one minute after activation, with further supporting observations provided by the stroboscopic experiments of Chauvaud *et al.* [7]. During this period of flagellar beating, sperm swimming speeds are slower, at just under 100μm/s and many turbot flagella are no longer significantly beating 80 seconds after activation [7, 12]. Hence turbot sperm do not progress more than about 1cm in their motile phase, in distinct contrast to the sperm of many mammals which must progress for at least tens of centimetres. More generally, even our preliminary considerations highlight that there is an enormous wealth of biodiversity and data in studies of fish sperm motility, in turn generating numerous novel modelling

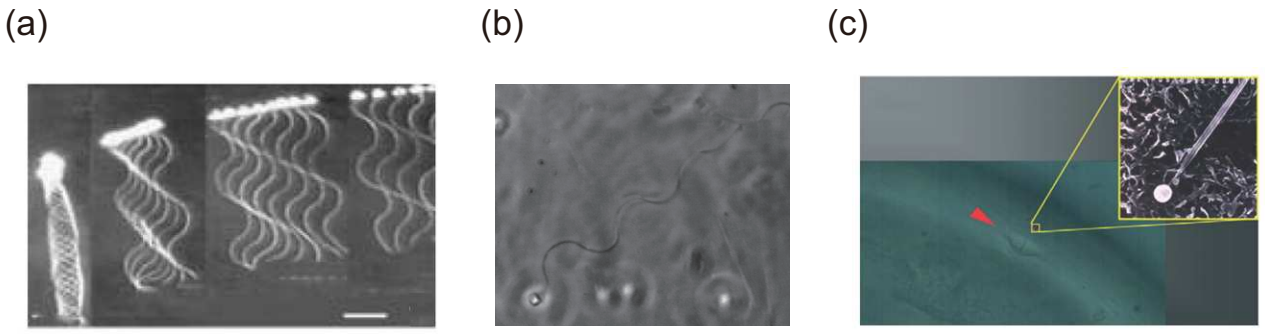

Figure 1: (a) Successive images of individual turbot spermatozoa obtained every 3 ms (from left to right in each) shortly after flagellar waveform activation; one can estimate the wavenumber is approximately 4π. Scale bar 10 microns. Reproduced from [9], with permission. Copyright, 2008, BioScientifica Ltd. (b) An unpublished image of a turbot sperm waveform observed one minute after activation; note that the distal beat pattern is extensively subdued and the wavenumber is slightly higher. (c) A turbot sperm adjacent to a turbot egg. Red arrow. The micropyle, which the sperm must reach and enter to fertilise the egg. Yellow box. The turbot sperm; note the difference in scales of the sperm and egg. Reproduced from [10], with permission.

questions from the perspective of the physical sciences. Within this larger framework, we will focus on an initial study of how the hydrodynamics of sperm motility can inform our understanding of the interactions between fish sperm and eggs, motivated by a fundamental question of sexual reproduction: how does a sperm find and then penetrate the egg?

To simplify the scope and the hydrodynamics, we will only consider pelagic eggs of teleost fish, which are buoyant, isolated and representative of natural fertilization for numerous commercial fish, such as turbot, sturgeon, carp and salmonids. Furthermore, sperm only enter these eggs via a micropyle opening, highlighted in Fig. 1c, which is small relative to the millimetre scales of the egg, so that simply reaching the egg is not sufficient. Certainly therefore, an ability for sperm to be captured by, and swim close to the egg surface, would be beneficial, in that the initial sperm-egg encounter region need not be limited to the micropyle. Furthermore, the presence of a surface is well-known to influence sperm motility with many species of spermatozoa observed to readily accumulate near a coverslip surface [43, 53]. This property is known as thigmotaxis and recent simulation studies have revealed that accumulation near a solid plane surface can be explained simply by hydrodynamic interaction between the cell and the surface [15, 46, 13, 48, 14, 27]. Furthermore, this behaviour has been reported in fish sperm studies, not only near a solid surface, but also near an air-water interface with reduced surface tension due to surfactant [11, 6]. In particular, given that the fish egg is approximately flat on the scale of a sperm, as highlighted by Fig. 1c, it has subsequently been hypothesized that thigmotaxis is a guidance cue in the fertilization of teleost fish pelagic eggs [10]. Our primary objective in this paper is therefore to test the physical feasibility of this hypothesis by employing a hydrodynamical study of fish sperm behaviour near a smooth spherical surface, representing the egg.

Nonetheless, and in contrast to the smooth micropylar region seen in Fig 1c and Fig 2b for turbot, some species' micropylae are ridged, as illustrated for *Apogon cookii* eggs in Fig. 2a, raising the prospect that surface topography may also assist sperm guidance, which is for future study. In addition, chemotaxis is certainly observed as a navigation cue for sea urchin sperm, as initially reported by Miller [37] and recently reviewed by Alvarez et. al. [2]; in contrast, the presence of fish sperm chemotaxis is uncertain

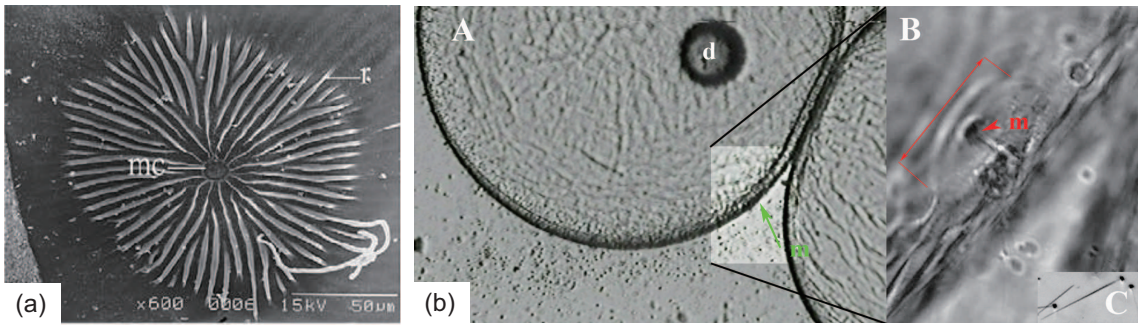

Figure 2: An illustration of the ridge structures in the micropylar region of *Apogon cookii* eggs: (mc, micropylar channel, r, ridge, scale-bar: 50 microns); reproduced from Chen et. al. [8], with permission. (b) An unpublished image of a turbot egg, its micropyle and a turbot spermatozoon. Left (A): turbot egg (about 580μm radius) with lipid droplet (d) and micropyle (m, green arrow). Right (B): enlarged portion of the lighter rectangle with micropyle (m, red arrow head), a funnel shaped canal about 3μm diameter at entrance, surrounded by a circular depression (double arrowed segment). Tangential view, optical video-microscopy using 100X lens phase contrast optics. Bottom right inset (C): immotile turbot spermatozoon about 45 μm total length at the same scale as (B).

in general, with only limited evidence for salmonid and herring in the local vicinity of the micropyle [55]. Consequently, we will assume the absence of chemotaxis in our studies below on the grounds it is not established in most fish and also that the proof of principle for chemotactic guidance is already clear from sea urchin studies, whereas our focus is a proof of principle as to whether thigmotaxis can assist in fish sperm navigation to the egg micropyle. Thus, we use observed turbot flagellar waveforms for fish sperm swimming near a surface, as illustrated in Fig. 1, to explore whether such flagellar waveforms will also result in sperm recruitment and retention by a smooth spherical surface, with a radius taken from the observed range for fish eggs. In addition, such results, together with simulations of human sperm near smooth spheres, will enable us to explore a secondary objective, which is to assess whether the dynamics of sperm near a large spherical surface can be approximated by that of a plane and hence also constitutes an initial modelling study of sperm thigmotactic sensitivity to changes in surface geometry.

2 Models and Methods

We document the mathematical representation of sperm swimming towards and adjacent to a fish egg, taking initial parameters primarily from observations of mid-season turbot eggs and turbot sperm in the early stage of activation, as summarised in Table 1, before generalizing to consider different scenarios. The kinematic problem for predicting the trajectory of a sperm requires a specification of both the sperm head and the flagellar beat pattern, as described below, prior to a summary of the fundamental biophysical equations governing the spermatozoan trajectory and the numerical algorithm used to solve these equations.

Parameter	Interpretation	Value	Source
R	Turbot Egg radius	$488 - 520\mu$m	[30]
R	Salmon Egg radius	≈ 3mm	[3]
c	Sperm head radius (turbot)	1.7μm	[50]
a	Flagellar radius	0.1μm	[51]
L	Flagellar length	43μm	[51]
kL	Wavenumber	4π	Fig. 1a and [9]
A	Flagellar envelope parameter	0.02	Fig. 1a and [9]
B	Flagellar envelope parameter	$0.05L$	Fig. 1a and [9]
ω	Angular frequency	60Hz	[9]

Table 1: Reference parameters for the fish sperm flagellum with a beat pattern in the early stage of activation, together with reference egg sizes. Note that the sperm parameters are typically based on observations of turbot [9, 50, 51] immediately after activation, as occurs on contact with higher osmolarity solution [7], such as seawater. The lower egg radius corresponds to the range for mid-season turbot eggs plotted in Fig. 1 of Jia *et al.* [30] though the variability with the stage of the season is not significant for our purposes, with early and late season eggs possessing radii in the range $560 - 605\mu$m [30]. Finally, the larger egg radius is based on salmon [3] and throughout all simulations we take the viscosity, μ, to be given by that of water, $\mu = 0.01$g/[cm·s].

2.1 The virtual egg, sperm head and flagellum

The egg is a sphere, with a range of diameters ranging from 1mm, reflecting the size of turbot, sea-bass and red tuna eggs to 6mm, for large salmon. The turbot, used as model species in this paper, has a typical egg radius among the large diversity of fish egg size [1]. In the simulations below, the egg possesses a smooth and rigid surface, whilst its centre is fixed at the laboratory frame origin, as the force exerted on the egg by sperm beating is negligibly small compared to that required to move the egg at any significant speed.

Unless explicitly stated otherwise, the virtual sperm cell head is modelled as a sphere and taking the sphere radius to be $c = 1.7\mu$m is an excellent representation of the turbot sperm head geometry [50]. Virtual sperm heads which are prolate ellipsoids, with the head-flagellum junction at the pole of the major axis, are also considered very briefly below since some fish, such as sturgeon, have sperm that possess highly elongated heads [39].

The virtual sperm flagellum is assumed to be a cylindrical tube, with length $L = 43\mu$m and radius $r = 0.1\mu$m [51], as shown in Fig. 3. We should note that the turbot flagellum also possesses sidefins, as observed in many fish spermatozoa [51], though we do not take such complexities into account, observing that the dynamics of a slender-body with non-circular cross-section can be approximated by a slender body with a circular cross section of the same perimeter [4]. We also briefly consider simulations of virtual human sperm near spheres, with the cell parameters of Table 3 and the details of the associated parameter estimation can be found in Ishimoto and Gaffney [27].

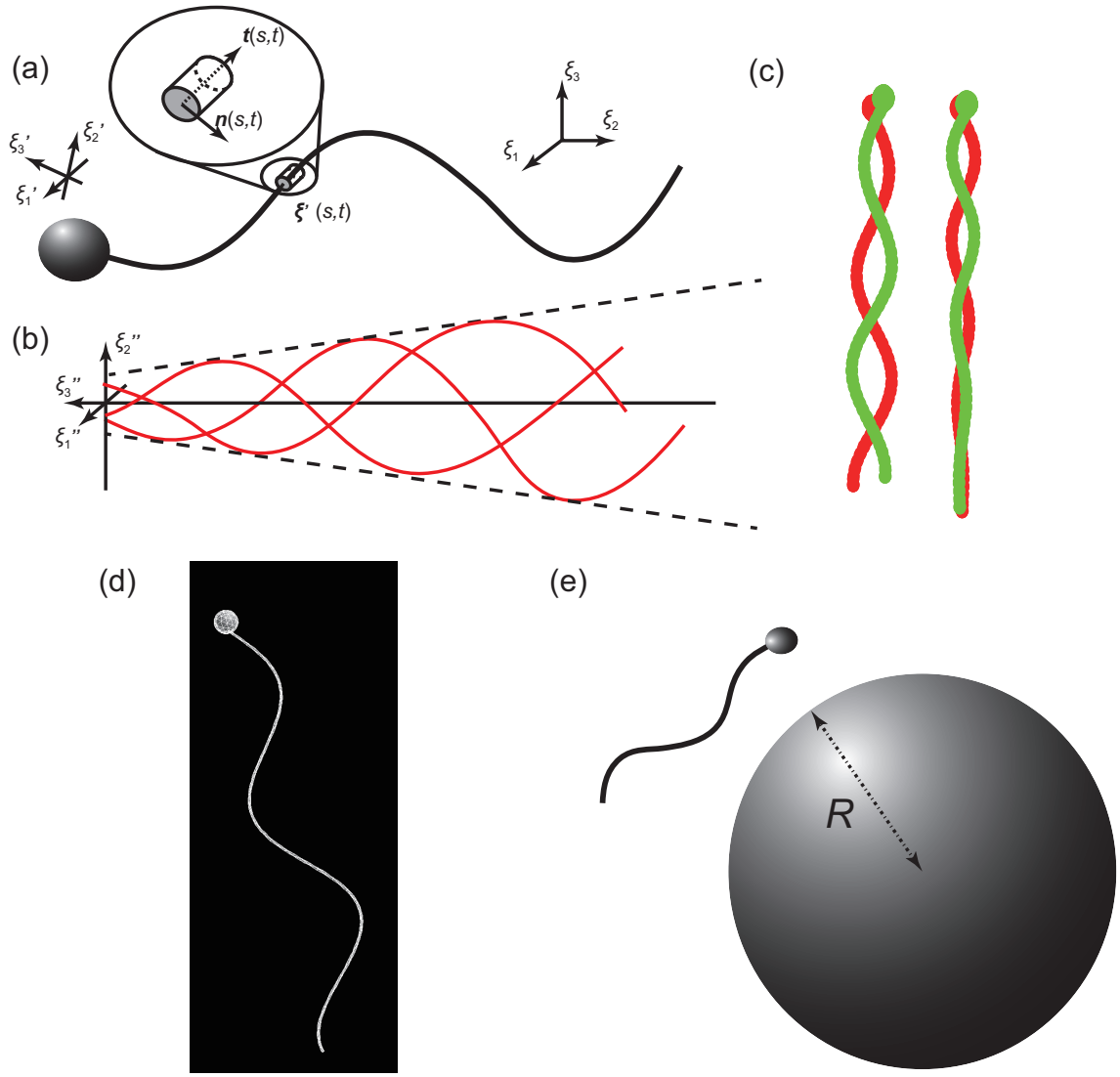

Figure 3: A schematic picture illustrating the parameterisation of a virtual spermatozoan flagellar wave and the associated reference frames. (a) The inertial frame, $\boldsymbol{\xi}$, is depicted with the sperm head fixed frame, $\boldsymbol{\xi}'$, and a schematic of the sperm head and flagellum, including the unit tangent and normal vectors of the flagellum. (b) The flagellar beat pattern is depicted in the flagellar frame $\boldsymbol{\xi}''$ at snapshots of time; at any instant in time, the resulting flagellum is translated and rotated such that it joins the sperm head at its connection with the flagellum, as detailed in section 2.1.2. (c) Images of the early stage, left, and late stage, right, flagellar beat patterns of virtual turbot sperm at opposite phases of the flagellar beat cycle (red vs. green) with *prescribed bending* conditions at the head-flagellum junction, as detailed in section 2.1.2. (d) A snapshot of the meshed early-stage virtual turbot sperm flagellar beat, with *prescribed bending* conditions for the connection between the sperm head and flagellum. (e) A schematic picture of the swimming sperm near an egg, though the egg and sperm are not to scale. The egg is considered as a smooth rigid sphere with radius R. Figures (a), (b) are reprinted with amendments, from Ishimoto and Gaffney [27], with permission.

Parameter	Interpretation	Value	Source
a	Flagellar radius	0.1μm	[51]
L	Flagellar length	43μm	[51]
kL	Wavenumber	5π	Fig. 1b and [7]
A	Flagellar envelope parameter	-0.05	Fig. 1b
B	Flagellar envelope parameter	$0.05L$	Fig. 1b and [7]
ω	Angular frequency	20Hz	[12]

Table 2: Reference parameters for the turbot fish sperm flagellar waveform for late stage motility, between about 40-80 seconds after activation, using Fig. 1b as a guide as well as data from the late-stage motility observations of Chauvaud et. al. [7] and the late stage controls of Dreanno *et al.* [12]. Note that the reduction in frequency with late stage motility does not alter the sperm trajectory due to the effective absence of inertia in sperm swimming.

Parameter	Interpretation	Value
V	Sperm head volume	7.36 μm^3
a	Flagellar radius	0.125μm
L	Flagellar length	56μm
kL	Wavenumber	3π
A	Flagellar envelope parameter	0.1087
B	Flagellar envelope parameter	$0.0543L$
ω	Angular frequency	14Hz

Table 3: Reference parameters for the human sperm flagellum and its beat pattern, with the parameter estimation as detailed in [27].

2.1.1 Flagellar beat pattern

The flagellar beat is taken to be a planar sinusoid, as illustrated in Fig. 1a,b. The fact such sinusoid waveforms are regularly observed entails that they are not sensitive to experimental conditions, which we note to justify the assumption below that the flagellar waveforms are not perturbed by the subtle changes in viscous drag experienced by the sperm as its distance from the egg varies. As in Smith *et al.* (2009b) we introduce three reference frames: the laboratory frame ($\boldsymbol{\xi}$), the cell-fixed frame ($\boldsymbol{\xi}'$), and the flagellar frame ($\boldsymbol{\xi}''$). In particular, if the sperm head is a prolate ellipsoid, rather than a sphere, the ellipsoid major axis is taken to lie on the ξ_3' axis of the cell fixed frame, as depicted in Fig 3a. Furthermore, the description of the centre curve of the flagellum (Fig 3a,b) is given by a function of the arc length, $s \in [0, L]$, from the head-tail junction, via

$$\boldsymbol{\xi}''(s,t) = \left(0, \xi_2''(\xi_3''(s,t)), \xi_3''(s,t)\right), \tag{2.1}$$

where the function ξ_2'' is given by

$$\xi_2'' = (-A\xi_3'' + B)\sin\left(k\xi_3'' + \omega t\right), \tag{2.2}$$

with the coordinate ξ_3'' implicitly determined as a function of arc length, via

$$s(\xi_3'') = \int_{\xi_3''}^{0} \sqrt{1 + \left(\frac{\mathrm{d}\xi_2''}{\mathrm{d}\tilde{\xi}_3''}\right)^2}\, \mathrm{d}\tilde{\xi}_3''. \tag{2.3}$$

This waveform corresponds to a linearly enveloped sinusoidal beat, which is the form observed for many fish sperm, in particular turbot as highlighted in Fig. 1a,b. For early-stage activated turbot sperm the beat frequency is taken to be $\omega = 60$Hz [9], whilst 20Hz is used for late stage turbot sperm [12], though note that the swimming trajectory of spermatozoa is independent of the beat frequency as sperm swim with effectively zero inertia. For early stage flagellar beating, we take the beat parameters A, B, to respectively be 0.02, and $0.05L$, whilst the wavenumber k is given via $kL = 4\pi$, as estimated from Fig 1a, which in turn is taken from Cosson et al. [9]. In contrast, for late stage activation the flagellar beat parameters of Table 2 are used, as estimated from Fig. 1b. Finally, note that in either stage the sperm progresses 3mm or more, since it spends at least 30 seconds swimming at more than $150\mu\mathrm{ms}^{-1}$ in the early stage and about 40 seconds at more than $80\mu\mathrm{ms}^{-1}$ during the late stage of the beat pattern; hence the sperm travels at least 70 flagellar lengths, $70L$, in each phase which is not shorter the trajectories presented in the result sections, and hence we do not detail the transition between the beat patterns in the simulations.

2.1.2 The head-flagellum connection conditions

Fixed conditions The details of the connection between the flagellum and the sperm head need to be specified. One possibility we consider are *fixed connections*, whereby the head surface and the proximal flagellum are fixed at right angles. Thus the relationship between the head-fixed frame and flagellar frame is a translation and rotation that can be determined from the flagellar waveform, such that the curve representing the flagellum in the head fixed frame, $\boldsymbol{\xi}'(s)$, firstly satisfies

$$\boldsymbol{\xi}'(s=0) = \mathbf{0}.$$

This ensures that the flagellum always connects to the same material point on the sperm head surface, which is on the major axis of the sperm head if a prolate ellipsoid is considered rather than a sphere. The second condition is that

$$\frac{\mathrm{d}\boldsymbol{\xi}'}{\mathrm{d}s}(s=0) = (0,0,-1),$$

so that the proximal flagellum is always at a right angle to the sperm head. In addition, the head-fixed frame of the sperm is related to the laboratory frame, with respect to which observations are made, via a further translation and rotation though these latter transformations must be found together with the sperm swimming trajectory and are not known a priori.

Prescribed bending conditions The above *fixed* connection conditions are typically the only ones considered in modelling mammalian sperm due to an extensive mid-piece and proximal accessory structures [17], though these are generally absent in fish, as illustrated by the electron microscopy of Siberian sturgeon sperm, which reveals a mid-piece of only a micron in length, which is effectively part of its 5 micron long cell body [39]. Hence we also consider *prescribed bending conditions*. The first of these conditions is

$$\boldsymbol{\xi}'(s=0) = \mathbf{0},$$

so that the flagellum always connects to the same material point on the sperm head surface, as above. The second condition is that the ξ_3' axis of the sperm head frame is parallel with the ξ_3'' axis of the flagellar frame. Hence the tangent vector of the flagellum at its most proximal point, relative to the flagellar frame, $\mathrm{d}\boldsymbol{\xi}''(s,t)/\mathrm{d}s$ at $s=0$, is equal to the tangent vector of the flagellum at its most proximal point, relative to the cell-fixed frame, $\mathrm{d}\boldsymbol{\xi}'(s,t)/\mathrm{d}s$ at $s=0$, i.e.

$$\frac{\mathrm{d}\boldsymbol{\xi}'}{\mathrm{d}s}(s=0,t)=\frac{\mathrm{d}\boldsymbol{\xi}''}{\mathrm{d}s}(s=0,t).$$

In other words, the sinusoid in the flagellar frame is simply specified to be translated to the origin in the cell fixed frame, without rotation.

An example of a virtual turbot sperm flagellum beat at a snapshot in time for *prescribed bending* conditions at the head flagellum junction is given in Fig 3d, whilst extensive flagellar bending at the sperm-flagellum connection, as consistent with these *prescribed bending* conditions, can be seen in Fig. 1a. Note that more generally, extensive flagellar bending at the head-flagellum connection can be very clearly seen in the fine detailed population level characterisation of the waveform associated with sea urchin sperm [42], which is another example of marine sperm whose flagella lack the proximal accessory structures of mammalian sperm.

2.1.3 Surface Forces

As a virtual sperm approaches an egg surface, the numerical meshes required to resolve the dynamics have a gridsize that becomes extremely small, and thus the numerical simulation cannot be proceed. Furthermore, in such a situation, the distance of approach entails that molecular scale surface interactions between the cell and the egg surface, such as those due to van der Waal forces, must be considered. Measurements of the molecular scale interaction potential energy have not been reported for sperm, though studies of *E. coli* highlight non-trivial surface-cell interactions at separations on the scale of tens to one hundred nanometres [34]. However, the details are complex, depending on the surface and the solute; for instance in human sperm experiments with glassware, the tendency of cells to stick to glass can be reversed by adding dilute serum albumin [47], presumably converting attractive surface forces into repulsive surface forces. Furthermore, these surface interactions are not captured by the simplest, DVLO, theory at physiological osmolarity, as explicitly demonstrated for yeast cells [44].

Hence, there is no clear quantitative form to use for the surface interaction, though we assume it is repulsive rather than attractive, to prevent sperm-egg sticking which is consistent with observation of sperm swimming across an egg surface [10, 54]. Thus, in section §4.3 below, we utilise a simple repulsive interaction, as considered in previous modelling studies [13, 29]. In particular, here we specifically take the force per unit area of the sperm cell surface given as a function of r, the distance from the egg surface, via

$$\boldsymbol{f}_{rep}(\boldsymbol{x})=g\frac{e^{-r/d}}{1-e^{-r/d}}\boldsymbol{e}_r, \tag{2.4}$$

with $\boldsymbol{e}_r$ the outward unit normal of the egg, and where g and d are constants. Once the parameter g is sufficiently large, the surface interaction will simply prevent the cell from entering the region within a distance $r \lesssim d$ of the surface. With μ denoting the fluid viscosity, we ensure we are in this regime by taking $g=200\omega\mu$, which is two orders of magnitude greater than the dimensional scales of force per unit area, $\omega\mu$. Below, we always use the viscosity of water, $\mu=0.01$g/[cm·sec], though

the value of the viscosity does not change the swimming trajectory in our model. The parameter d is typically given by $d = 0.01L = 430$nm for the virtual sperm simulations, though much smaller values of d are briefly considered below when considering sperm swimming adjacent to turbot eggs. This highlights that these modelling results are independent of the details of the surface repulsion, noting that quantitative surface potential data is highly contingent on the system details and thus not available. Nonetheless, with the simple potentials used here, virtual sperm cell simulations have previously matched observed behaviours, as illustrated in the supplementary information of Ishimoto and Gaffney [29].

3 Numerical scheme

The core numerical codes underlying the boundary element algorithms used below have built on the BEMLIB library accompanying Pozrikidis' text [38], with validation against exact results presented elsewhere, for instance the surface scattering of a squirmer [26, 49] and the efficiency of a large wavenumber spherical ciliate squirmer [28]. Further qualitative validation, with a comparison against observed sperm trajectories, is also presented in the supplementary material of Ishimoto and Gaffney [29]. Finally, observational and theoretical studies highlight that computational hydrodynamics can predict sperm swimming velocities [20, 18], demonstrating the proof of principle that modelling can predict, and thus contribute to the understanding of, sperm swimming.

3.1 Mesh generation

Numerically, the flagellum is interpolated by a hexagonal tube, with 'semi-spherical caps', following Shum et al. [45] where a swimming bacterium with a rigidly rotating prokaryotic flagellum is examined. The spherical sperm head is generated by the BEMLIB library accompanying Pozrikidis [38], with two mesh generation iterations. The head and the tail are separated by a distance of $0.05c$, where c is the sperm head radius, to avoid overlapping meshes and the meshes on the flagellar surface are generated around the circular cross section at each point along the flagellar centreline, as illustrated in Fig 4. Together with the head part, the total number of mesh points for the discretisation of the whole sperm cell surface is $N = 494$.

3.2 Boundary integral equation

The microscale flows associated with sperm swimming in a Newtonian fluid, such as water, are governed by Stokes equations, enabling the use of the single layer formalism of the boundary element method. This relies on the fact that the velocity field associated with the deforming swimmer, $\boldsymbol{u}(\boldsymbol{x_0})$, can be written in the boundary integral form in the inertial frame

$$u_i(\boldsymbol{x}_0) = -\frac{1}{8\pi\mu}\int_S G_{ji}(\boldsymbol{x}_0, \boldsymbol{x}) q_j(\boldsymbol{x})\, \mathrm{d}S_{\boldsymbol{x}}, \tag{3.1}$$

for $i = 1, 2, 3$, given volume conservation of the swimmer [28], with S representing the surface of the cell head and flagellum. The integral kernel G_{ij} is the Stokeslet in the presence of an external rigid sphere [23], and the Blakelet [5] for the simulation of swimming in the presence of an infinite rigid

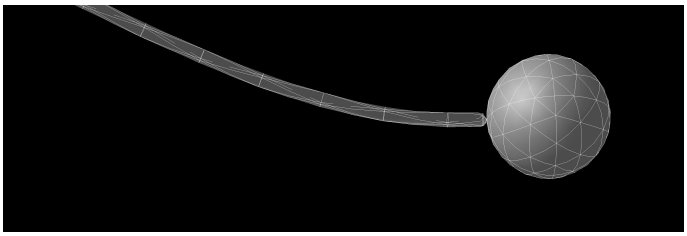

Figure 4: An illustration of the boundary element mesh.

plane wall, as shown in Fig. 7, whilst $\boldsymbol{q}$ denotes the unknown difference of the internal and external traction, and μ is the fluid viscosity.

As a consequence of the no-slip boundary condition, this boundary integral is imposed on the mesh-points. The surface velocities in the inertial frame are known in terms of the flagellar movement, that is the specification of the flagellum in the flagellar frame, the known translation and rotation mapping the flagellar frame to the cell fixed frame, and the mapping between the cell-fixed frame and the inertial frame, which is readily expressed in terms of the six scalar a-priori unknowns, the velocity $\boldsymbol{U}$ and angular velocity $\boldsymbol{\Omega}$ of the head-flagellum junction. The further unknowns are the tractions, $\mathbf{q}$, at each mesh point. Hence there are $3N + 6 = 1488$ scalar unknowns; enforcing the boundary integral 3.1 on each mesh point of the surface of the sperm cell gives $3N$ constraints. The final six scalar constraints are that the cell swims subject to zero total force and torque, as a consequence of the inertialess limit of Stokes flow, which yields:

$$\mathbf{0} = \int_S [\boldsymbol{f} + \boldsymbol{f}_{rep}] \, \mathrm{d}S_{\boldsymbol{x}} = \int_S \boldsymbol{\xi}' \wedge [\boldsymbol{f} + \boldsymbol{f}_{rep}] \, \mathrm{d}S_{\boldsymbol{x}}, \tag{3.2}$$

where $\boldsymbol{f}_{rep}$ is given by equation (2.4). The resulting $3N + 6$ scalar equations are linear and are solved via a singular preconditioning [38] and a subsequent an LU factorisation. This yields the tractions and, in particular, the cell velocity $\boldsymbol{U}$ and the cell angular velocity $\boldsymbol{\Omega}$.

3.3 Trajectory Determination

Given $\mathbf{U}$, $\boldsymbol{\Omega}$ then one can update the location of the sperm and its orientation in the inertial frame, allowing the determination of $\mathbf{U}$, $\boldsymbol{\Omega}$ at the next timestep, and hence a simple Euler iteration that would generate the virtual sperm trajectory. In practice the Heun method is much more efficient for the time stepping and has been implemented, similarly to previous works [26, 27, 28], with the numerical computations executed using the cluster system at the Research Institute for Mathematical Sciences (RIMS), and the Institute for Information Management and Communication (IIMC), Kyoto University. Further details on these numerical schemes can be found in Ishimoto and Gaffney [27] and we proceed to explore theoretical predictions from these simulations for sperm behaviour near a fish egg.

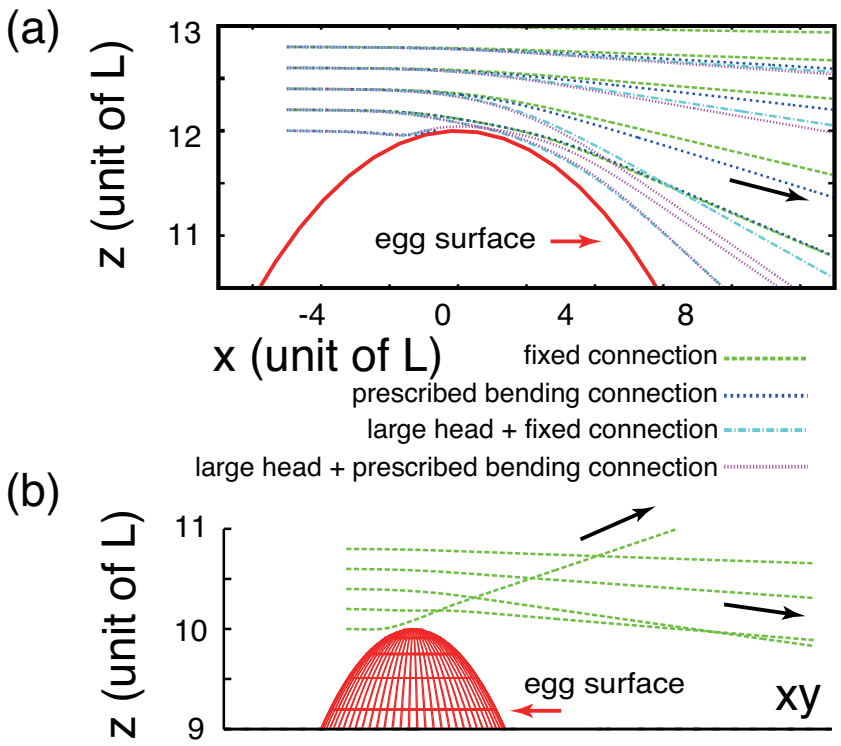

Figure 5: Simulations of sperm approaching an egg. (a) The trajectories presented are for the turbot sperm parameters of Table 1, with an early stage beat pattern, an egg radius of $12L$ and with both *prescribed bending* and *fixed* conditions at the head-flagellum junction. The large head simulations have doubled the size of the spherical turbot sperm head to 3.4μm in radius. Also, the lowest trajectories have also been initiated on a collision course with the egg surface. (b) A virtual human sperm, with the parameters of Table 3 and a *fixed* connection, swims towards a sphere of radius $R = 10L = 560\mu$m. Note that the sperm initiating on the lower trajectory is on a collision course with the sphere, but is eventually scattered.

4 Results

4.1 Collision Cross section

We first all consider the extent to which hydrodynamic interactions influence the trajectory of a sperm as it swims towards the egg from a distance, whilst not on a collision course, and thus we do not consider surface interactions at this stage. In particular, the influence of hydrodynamic interactions can be characterised by the egg collision cross section which is increased relative to the geometric cross section to account for the fact hydrodynamic interactions between a sperm and an egg are attractive.

4.1.1 Smaller egg sizes

In Fig. 5a the sperm and egg are nominally that of turbot with an egg radius of $R = 12L = 516\mu$m, within the range reported for mid-season turbot eggs [30]. The virtual sperm possesses an early stage

flagellar beat pattern, as characterised by the parameters of Table 1 and either *fixed* or *prescribed bending* conditions between the sperm cell body and the flagellum. In addition, the sperm head is a sphere of radius c or $2c$, where the larger radius corresponds to the large head trajectories of Fig. 5a.

As initial positions for the trajectories, we set $x = -5L$, and $z - R = 0.0L, 0.2L, \cdots, 0.8L$ with the sperm directed along the x axis with a horizontal beat plane, as seen in Fig. 5a, whilst the egg is centred at the origin. In the absence of sperm-egg hydrodynamic interaction z would be conserved on these trajectories, at least until sperm-egg collision for the lowest initiated trajectories. However, the results of the numerical simulation in Fig. 5a highlight that the sperm trajectories curve towards the egg since the cells are weakly attracted by the egg surface via hydrodynamic interactions. However, this hydrodynamic influence is insufficient to capture the cells around the egg, but instead induces a scattering of spermatozoa. In particular, the surface induced enhancement of the collision cross-section of the egg is less than that associated with a sphere of radius $12.2L$, i.e. an 8.6μm increase, and thus less than the observed variation in turbot egg radius (Table 1 and Jia *et al.* [30]).

Consequently, the observation that the egg collision cross section is essentially unaltered is predicted to be robust to parameter variation. In particular, this modelling observation also holds for the prolate ellipsoid sperm head geometry described in section 2.1 for aspect ratios of the major to minor sperm head axes of up to 4 (results not shown), at least for parameter regimes where the flagellar wave broadly corresponds to that of turbot. This is also further reinforced by Fig 5b, where sperm with the human parameters of Table 3 and not on a direct collision course with a sphere of radius $10L = 560\mu$m, are again only weakly scattered.

4.1.2 Larger Egg Sizes

In Fig. 6, virtual turbot sperm, with the early stage beat pattern parameters of Table 1, and the *prescribed bending* connection are considered as they swim towards a larger egg, with radius of $R = 50L = 2.15$mm. Analogously with the above numerical simulations, each sperm is initially located at $x = -5L$ and $z - R = 0.2L, 0.4L, \cdots, L$. One can see that hydrodynamic interactions do attract the sperm towards the egg and they eventually approach the surface sufficiently closely that surface interactions must also be considered to understand the dynamics. Nonetheless, the increase in the collision cross section is still less than that associated with a relative increase of about 1% in the diameter; these simulations also highlight that understanding sperm dynamics near fish eggs necessitates the inclusion of surface interactions due to the very close approach of sperm to the egg.

4.2 The behaviour of sperm on a collision course

In either plot of Fig. 5, the lowest initial sperm trajectories place the sperm on a direct collision course with the egg. Scattering still occurs for the purple trajectory in Fig. 5a, which corresponds to a virtual turbot sperm with the early activation stage waveform and the parameters of Table 1, except for a sperm head of twice the radius. In the same plot, the early activation stage virtual turbot sperm, represented by the blue trajectory on a collision course, is observed to approach the egg on the scales where molecular surface interactions come into play and would crash into the surface if these were attractive. The latter is perhaps not that surprising in that the virtual turbot sperm also crashes into a flat plane in the absence of surface forces if it approaches it too closely (not shown). However, note in the lower plot, Fig. 5b, that when a virtual human sperm, as characterised by the parameters of

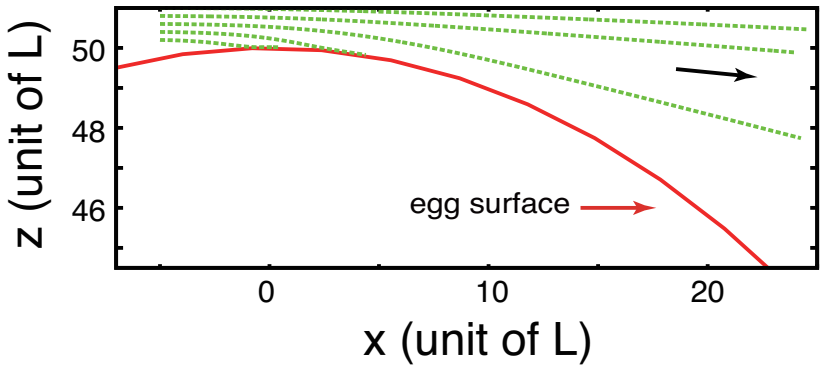

Figure 6: Large egg simulations. In the above the reference parameters of turbot sperm presented in Table 1 are used, with the *prescribed bending* connection. However, the egg radius is $50L = 2.15$mm, which is on the scale of salmon eggs.

Table 3, is placed on a collision course with an egg of radius $10L \approx 560\mu$m, that is 10 sperm lengths, extensive scattering occurs. This is despite that such a sperm swims stably adjacent to a plane, as highlighted in previous work [27].

Hence, the simulations for human sperm further highlight that stable swimming adjacent to an egg an order of magnitude larger than a sperm cell is not guaranteed simply by the observation of stable boundary swimming near a plane. More generally, these numerical observations indicate that the capture of sperm by the egg is by no means automatic, even with an initial collision course, and further emphasise the need to consider the influence of surface molecular interactions, as we now pursue.

4.3 Boundary Accumulation Via a Repulsive Surface Interaction

In Fig. 7 we introduce the repulsive surface interaction of equation (2.4) for virtual turbot sperm with the early stage beat pattern parameters of Table 1, swimming near a plane; we see that stable swimming now emerges, with the head-flagellum junction about 4 microns above the plane. However, this may not be sufficient to ensure stable swimming near a sphere an order of magnitude larger in lengthscale than the sperm, as seen above for virtual human sperm simulations. This is indeed the case, as observed in Fig. 8a, where the repulsive interaction acts to align the virtual turbot sperm along the surface with an extended, but ultimately transient, surface swimming before the sperm eventually escapes from the egg. In Fig. 8c, almost identical trajectories are observed for virtual sperm which differ due to the use of late stage turbot flagellar beat parameters, as presented in Table 2. This therefore highlights that the late stage transition in the turbot sperm beat to a flagellar waveform which is distally suppressed and with higher wavenumber does not prevent, or ameliorate, the predictions of transience near turbot-sized fish eggs. Similarly, reducing the surface force interaction lengthscale parameter d in equation (2.4) to $d = 43$nm also does not significantly alter the trajectories (figure not shown), illustrating that the details of the surface force also do not ameliorate the predictions of transience near turbot-sized fish eggs.

However, once the egg radius is sufficiently large, stable surface swimming occurs, as seen in Fig. 8b for turbot sperm in the early stages of activation near an egg of radius $50L \approx 2.15$mm, which is

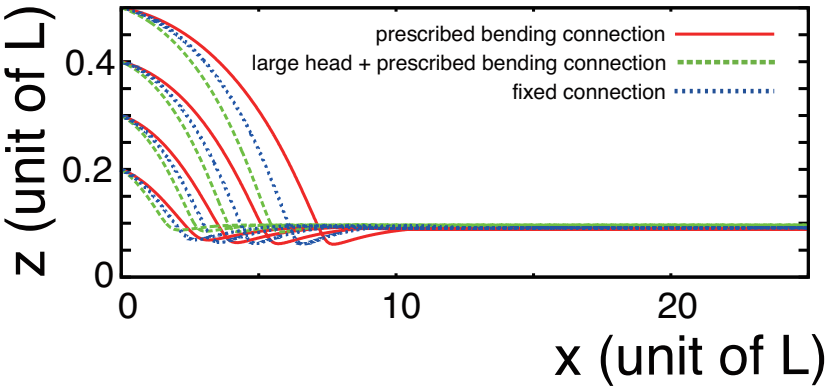

Figure 7: Trajectories near a flat plate for a virtual turbot sperm with the early activation stage beat parameters given in Table 1 and the presence of the repulsive surface interaction, equation (2.4). Results are plotted for different head sizes and head-tail connection conditions, with the sperm initially located parallel to the xy plane at a range of distances from an infinite plane wall at $z = 0$. The sperm eventually enter the region where the surface repulsion force are significant and then ultimately swim stably near the wall.

approaching the radius of a salmon fish egg. The predictions associated with swimming near a sphere the size of a turbot egg are inconsistent with observations given that turbot sperm do swim adjacent to turbot eggs. Nonetheless, a propensity for for stable near-egg swimming is clear and it is the quantitative details that do not align precisely with observation. In addition, the mechanics is different from that predicted for the stable swimming of a virtual human sperm near a plane, which does not require any surface interaction [46, 27].

4.4 A further inspection of stable versus transient sperm swimming near a sphere

Since the transition to stable sperm swimming near an egg occurs at a larger sphere radius than observed, we proceed to examine the model predictions of transient versus stable swimming in more detail, via Fig. 9. Here, the time course for the distance between the sperm head-tail junction and the sphere surface is plotted, together with the angle of the sperm head orientation to the tangential plane of the sphere, as depicted and detailed in Fig. 9a. In particular, the virtual turbot sperm has an early activation stage waveform with a parameterisation via Table 1; in addition it starts at $x = -R$ and $z = 15L$ with an initial velocity in the positive $+x$ direction and thus swims towards a spherical egg, which has a radius of either $R = 43L$ or $R = 44L$. Finally, different values of g and d, respectively the strength and lengthscale of the repulsive force are considered, with plots presented for

$$(g/\omega\mu, d/L) \in \{(200, 1/100), (200, 1/200), (400, 1/100)\} .$$

The first two plots of Figs. 9b,c with the reference surface repulsive potential parameters, $(g/\omega\mu, d/L) = (200, 1/100)$, demonstrate that the transition to stable swimming occurs within the range of sphere radii, $R \in (43L,\ 44L)$, i.e. about 2.5 times larger in radius than a turbot egg. Furthermore, the angle of these trajectories in Plot 9c demonstrate that sperm align with the sphere in a very similar manner, becoming oriented to swim away from the sphere, with the angle becoming positive. Nonetheless the angle is very small and hence the sperm swims close to the sphere for an extended period even if it

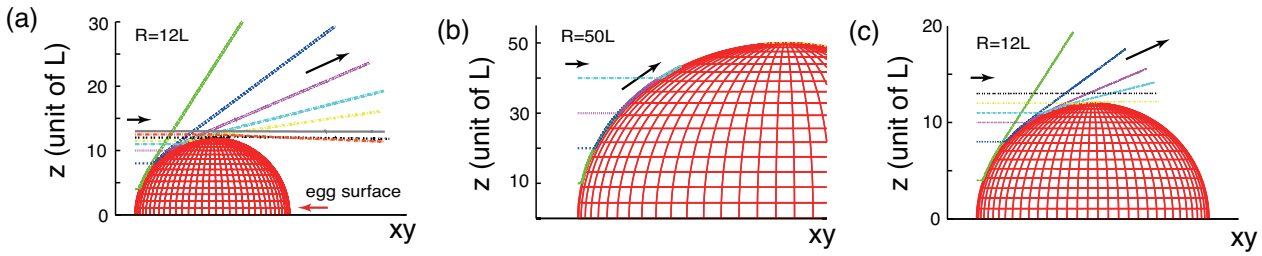

Figure 8: Trajectories of model turbot sperm with the *prescribed bending conditions* at the head-tail junction, swimming near an egg with radius $R = 12L$, and $R = 50L$, with the swimming direction given by the black arrows and the eggs depicted using a meshed spherical surface. (a) For a sperm exhibiting the early activation beat pattern of Table 1, there is no stable sperm surface swimming, even with surface repulsion forces for an egg radius of $R = 12L$. However an extended, albeit ultimately transient, surface swimming is observed. (b) With the early stage activation parameters for the flagellar beat pattern presented in Table 1, stable surface swimming can be observed for the virtual turbot sperm when the egg radius is $R = 50L = 2.15$mm. Here virtual sperm swim along the egg surface, and do not be separate from the egg. (c) One can observe that the trajectories are very similar for virtual turbot sperm with the late stage flagellar beat parameters of Table 2 and, in particular, that there is again only transient, albeit extended, swimming near the egg surface.

eventually leaves. In particular, the sperm is still under the influence of hydrodynamic attraction of the sphere, which is longer ranged than the surface repulsion potential. Hence the sperm starts to turn, though the hydrodynamic attraction is weak so the turning takes a significant number of beat periods. Whether the sperm swims stably, as with the green trajectory of Fig 9b, or transiently near the surface, as with the red trajectory, appears to hinge on whether the sperm turns sufficiently for it to be attracted back towards the egg. If it is, there is damped oscillation in the radial distance and the sperm swims stably near the egg. Otherwise, it drifts away, as in the red trajectory of Fig 9b. Note also that these observations occur for the blue and purple trajectories associated with further parameter choices in Fig 9b,c illustrating that this aspect of the dynamics is not specific to detailed parameter choices.

In summary, these plots illustrate that the question of whether the swimming near the egg is stable or transient is about a competition between two influences. The first is the small exit angle of the initial close-scale interaction of the sperm and the egg, which initiates a slow drift away from the egg. The second is the weak hydrodynamic force attracting the sperm back.

5 Discussion and Conclusions

In this study, we have considered the behaviour of virtual sperm swimming in the vicinity of smooth spherical fish eggs by modelling the mechanical interactions of a sperm with its surroundings, with the implicit assumption that mechanical feedback, such as the subtle change in viscous drag near a surface, does not alter the flagellar beat pattern. In particular, the first objective is to assess whether thigmotaxis, the presence of a surface acting as guidance cue, is active in the fertilisation of fish eggs, focussing on teleost fish pelagic eggs, which allows the simplifying assumption that the egg is buoyant and isolated.

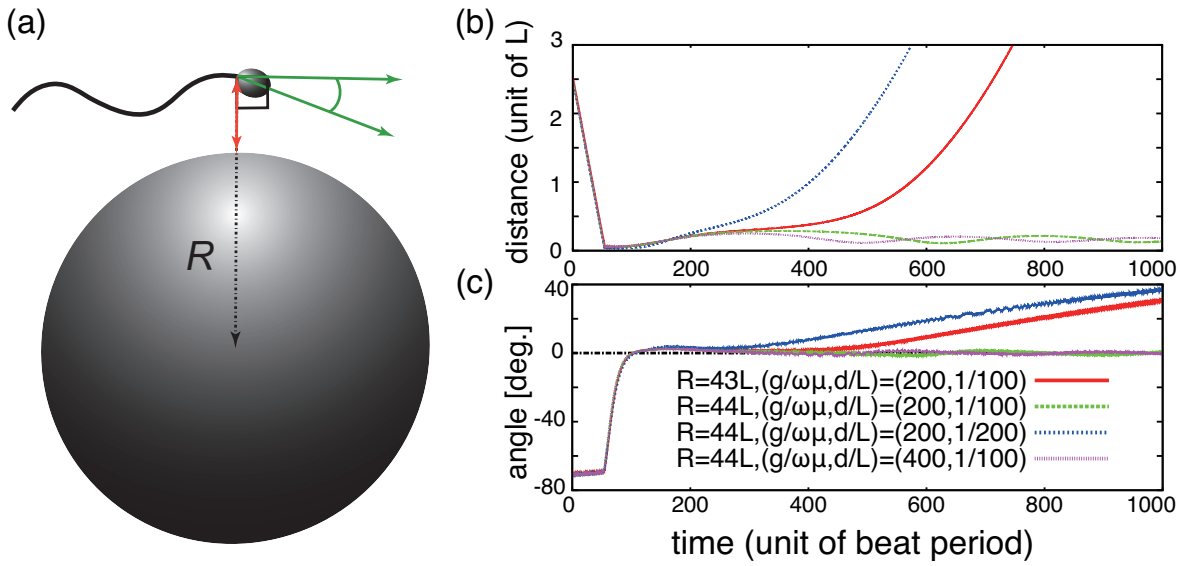

Figure 9: A detailed resolution of the temporal dynamics near a sphere for the virtual turbot sperm with the early activation stage waveform, as parameterised in Table 1 and with *prescribed bending conditions* at the head-tail junction. In particular, results are presented for an egg with a radius of $R = 43L$ and $R = 44L$, together with different parameter values for the surface repulsion force. (a) A schematic picture, not to scale, of the swimming sperm near an egg, illustrating the plotted parameters in (b) and (c). (b) Time evolution of the distance between the head surface and the head-tail junction for the model sperm, which corresponds to the magnitude of the red arrow in (a). (c) Time course for the angle of the sperm head orientation, as defined by the head axis of symmetry passing through the head-flagellum junction, with respect to the tangential plane of the egg surface, which is perpendicular to the red arrow of (a) and passes through head-flagellum junction. This angle is illustrated in green in (a).

We observe that sperm essentially not on a direct collision course would pass by the egg in the absence of other guidance cues, with the influence of hydrodynamical interactions inducing a change of the egg collision cross section which is smaller than that due to the natural variation in turbot egg size. Even for larger eggs, up to the sizes those observed for salmon, with radii of about 3mm, the relative increase in collision cross section radius due to hydrodynamic interactions is less than that associated with about a 1% change in egg diameter, as highlighted in Fig. 6. Consequently, the modelling predicts the physical guidance cue of thigmotaxis, or surface attraction, effectively plays no role in bringing sperm and the egg into contact, despite the large disparity of lengthscales between the gametes.

We proceed to consider what happens if a virtual sperm is on a collision course with the egg. With the absence of surface forces in the model, the sperm can still escape, as illustrated by the trajectories in Fig 5a for the larger sperm head, emphasising that the capture of sperm by an egg is by no means automatic. Nonetheless, the virtual turbot sperm is observed to crash into the surface, as illustrated in Fig. 5a and, more generally, surface crashing is also observed for these sperm in the vicinity of larger eggs, as shown in Fig. 6.

Such observations are consistent with the fact virtual sperm with turbot parameters would crash into a wall, rather than stably swim next to it due to just hydrodynamic forces. However, this hides the

fact the hydrodynamic interactions between a sperm and a sphere, such as a fish egg, are subtle. This is particularly emphasised in Fig. 5b where a virtual human-sperm, which swims stably next to a plane due to hydrodynamics alone [46, 27], is in fact scattered by a sphere when swimming into it on a collision course. Thus, in context of our second objective, of assessing whether sperm boundary accumulating behaviours can be sensitive to changes in surface geometry, we immediately see that one cannot generally infer results from simulations near a plane for the dynamics of sperm near a sphere with a radius that is an order magnitude larger than the sperm length. This is despite the fact that such a spherical egg might be approximated as a flat plane on the scale of a sperm cell and highlights an extensive sensitivity to the details of surface geometry.

As emphasised by Fig. 7, stable boundary accumulating behaviours for virtual turbot sperm adjacent to a plane can be induced by the inclusion of surface repulsion, which removes the tendency of sperm to crash into the surface. In particular, the presence of repulsive surface forces leads to the prediction that virtual turbot sperm transiently swim close to spheres the size of turbot eggs, crossing the egg surface for a couple of hundred microns; this also emphasises the geometric sensitivity of boundary swimming as near a plane this swimming is stable rather than transient. Furthermore, the detailed trajectories near turbot eggs are robust when considering simulations with greatly reduced surface potential lengthscales or with virtual turbot sperm possessing the flagellar beat pattern associated with late stage activation, more than about 40 seconds after motility is initiated.

However, it is important to note that the predicted transience of swimming near spheres the size of turbot eggs is not consistent with the observation that, in practice, turbot sperm swim stably adjacent to their eggs. In particular, spheres with radii of about a 1.8 millimetres or larger are required for predictions of stable surface swimming, as indicated in Figs. 8b, 9. Thus effectively, we have a disagreement between the modelling and observation; however it is with regard to the quantitative details, rather than the qualitative principles. Furthermore, inspection of Fig. 9 indicates that whether transient or stable swimming is observed is due to a competition between two driving influences, one is the small positive exit angle of the initial sperm-egg interaction causing the sperm to drift away from the egg; the second is the weak hydrodynamic attraction between the sperm and the egg. Hence the question of stability versus transience in sperm swimming next to a sphere may be sensitive to modelling approximations that induce small changes in the scattering angle or the hydrodynamic attraction. In particular, possibilities may include a combination of geometric sensitivity and the neglect of any subtle surface topography, such as a slight flattening of the egg near the micropyle, or a neglect of subtle 3D components of the flagellar beat pattern.

Furthermore, the modelling predicts that the combined influence of surface force repulsion with hydrodynamic attraction is the only prospect for the virtual turbot sperm to swim close to its egg, either stably or for extended but ultimately transient periods, without extensive biological feedback or additional physics. Nonetheless, even the transient egg-surface swimming functions as a reproductively beneficial guidance cue, keeping the sperm near the fish egg surface for a prolonged period, thus heightening the chances of an encounter with a micropyle.

More generally surface swimming due to the influence of both surface repulsion and hydrodynamic attraction, has been illustrated previously in investigating rheotactic guidance [29]. Furthermore, despite numerous previous studies, the results presented here highlight that sperm surface swimming is far from understood and immediately raise the interesting question of why sperm swimming behaviour is sensitive to surface geometry. In addition, the dynamics of how a sperm may behave once the micropyle is encountered is beyond the scope of this study, not least because the geometry is much more complicated at this point and hence the numerical schemes used here are not applicable. This

offers another very interesting area for further study, though there are also likely to be further biological complexities such as species specificity of sperm entry into the egg due to surface glycoproteins at the micropyle or, for some species, the prospect of chemotaxis local to the micropyle [54, 55].

In summary, we have studied simulations of virtual sperm approaching and swimming near an egg, observing that hydrodynamic interactions alone are inadequate to play any significant role in bringing sperm towards an egg, nor can such interactions maintain a virtual sperm swimming across a fish egg without additional physics or biology. Nonetheless, the incorporation of repulsive molecular scale surface interactions leads to predictions of turbot sperm swimming extremely close to an egg, albeit transiently for turbot sized eggs in contrast to observations of stable swimming, which is only realised in the modelling predictions with a larger egg size. Hence the predicted transience of virtual turbot sperm swimming near a model turbot egg only represents a detailed quantitative difference between modelling and observation. In particular, the transience arises when the small exit angle following the initial sperm-egg encounter is not compensated by the weak hydrodynamic sperm-egg attraction and thus the transition between stable swimming and transience may be particularly altered by modelling factors that impact on the exit angle or the hydrodynamic attraction, such as surface topography. Regardless, one has that the egg surface is predicted to be a guidance cue for sperm once they are sufficiently close. In addition, further studies are required for both mammal and fish sperm, to understand thigmotaxis in confined geometries. In particular, our observations imply that sub-millimetre surface geometries, and thus the scale of many microdevices for instance, can be insufficient to allow the legitimacy of planar surface approximations in general, upon which essentially all modelling and theoretical studies to date have been based upon.

Acknowledgements

The authors acknowledge the referee for the comments and feedback that have helped us enrich the paper. K.I. acknowledges JSPS for its fellowship and KAKENHI, grant-in-aid for a JSPS Fellow. Elements of these simulations have been performed using the cluster computing system within Research Institute for Mathematical Sciences (RIMS), and Institute for Information Management and Communication (IIMC), Kyoto University. Part of the studies by J.C. was financially supported by the Ministry of Education, Youth and Sports of the Czech Republic - projects "CENAKVA" (No. CZ.1.05/2.1.00/01.0024), "CENAKVA II" (No. LO1205 under the NPU I program) and COST (No. LD14119), by the Grant Agency of the University of South Bohemia in Ceske Budejovice (No. 114/2013/Z), and by the Czech Science Foundation (No. P502/15-12034S and GACR P502/12/1973).

References

[1] E. H. Ahlstrom and G. Moser. Characters useful in identification of pelagic marine fish eggs. *CalCOFI Rep.*, 21:121–131, 1980.

[2] L. Alvarez, B. Friedrich, G. Gompper, and U. Kaupp. The computational sperm cell. *Trends in Cell Biology*, 24:198–207, 2014.

[3] D. Aulstad and T. Gjedrem. The egg size of salmon *Salmo soar* in Norwegian rivers. *Aquaculture*, 2:337–341, 1973.

[4] G. K. Batchelor. Slender-body theory for particles of arbitrary cross-section in Stokes flow. *Journal of Fluid Mechanics*, 44:419–440, 1970.

[5] J. R. Blake. A note on the image system for a stokeslet in a no slip boundary. *Proceedings of the Cambridge Philosophical Society*, 70:303–310, 1971.

[6] S. Boryshpolets, J. Cosson, V. Bondarenko, E. Gillies, M. Rodina, B. Dzyuba, and O. Linhart. Different swimming behaviors of sterlet (*Acipenser ruthenus*) spermatozoa close to solid and free surfaces. *Theriogenology*, 79:81–86, 2013.

[7] L. Chauvaud, J. Cosson, M. Suquet, and R. Billard. Sperm motility in turbot, *Scophthalmus maximus:* initiation of movement and changes with time of swimming characteristics. *Environmental Biology of Fishes*, 43:341–349, 1995.

[8] C. Chen, C. Wu, K. Shao, and J. Yang. Chorion microstructure for identifying five fish eggs of apogonidae. *Journal of Fish Biology*, 71:913–919, 2007.

[9] J. Cosson, A. Groison, M. Suquet, C. Fauvel, C. Dreanno, and R. Billard. Marine fish spermatozoa: racing ephemeral swimmers. *Reproduction*, 136:277–294, 2008.

[10] J. Cosson, A. Groison, M. Suquet, C. Fauvel, C. Dreanno, and R. Billard. Studying sperm motility in marine fish: an overview on the state of the art. *Journal of Applied Ichthyology*, 24:460–486, 2008.

[11] J. Cosson, P. Huitorel, and C. Gagnon. How spermatozoa come to be confined to surfaces. *Cell Motility and the Cytoskeleton*, 54:56–63, 2003.

[12] C. Dreanno, J. Cosson, M. Suquet, F. Seguin, G. Dorange, and R. Billard. Nucleotide content, oxydative phosphorylation, morphology, and fertilizing capacity of turbot (*Psetta maxima*) spermatozoa during the motility period. *Molecular Reproduction and Development*, 53:230–243, 1999.

[13] J. Elgeti, U. Kaupp, and G. Gompper. Hydrodynamics of sperm cells near surfaces. *Biophys. J*, 99:1018–1026, 2010.

[14] J. Elgeti, U. B. Kaupp, and G. Gompper. Response to comment on article: Hydrodynamics of sperm cells near surfaces. *Biophys. J.*, 100:2321–2324, 2011.

[15] L. Fauci and A. McDonald. Sperm motility in the presence of the boundaries. *Bull. Math. Biol.*, 57:679–699, 1995.

[16] L. J. Fauci and R. Dillon. Biofluidmechanics of reproduction. *Ann. Rev. Fluid Mech.*, 38:271–394, 2006.

[17] D. W. Fawcett. The mammalian sperm. *Developmental Biology*, 44:394–436, 1975.

[18] B. Friedrich, I. Riedel-Kruse, J. Howard, and F. Julicher. High-precision tracking of sperm swimming fine structure provides strong test of resistive force theory. *Journal of Experimental Biology*, 213:1226–1234, 2010.

[19] E. Gaffney, H. Gadêlha, D. Smith, J. Blake, and J. Kirkman-Brown. Mammalian sperm motility: observation and theory. *Annu. Rev. Fluid Mech*, 43:501–528, 2011.

[20] E. Gillies, R. M. Cannon, R. B. Green, and A. A. Pacey. Hydrodynamic propulsion of human sperm. *Journal of Fluid Mechanics*, 625:445–474, 2009.

[21] E. A. Gillies, V. Bondarenko, J. Cosson, and A. A. Pacey. Fins improve the swimming performance of fish sperm: a hydrodynamic analysis of the siberian sturgeon *Acipenser baerii*. *Cytoskeleton*, 70:85–100, 2013.

[22] J. Gray and G. J. Hancock. The propulsion of sea urchin spermatozoa. *Journal of Experimental Biology*, 32:802–814, 1955.

[23] J. J. L. Higdon. A hydrodynamic analysis of flagellar propulsion. *Journal of Fluid Mechanics*, 90:685–711, 1979.

[24] M. Hines and J. J. Blum. Bend propagation in flagella I. Derivation of equations of motion and their simulation. *Biophysical Journal*, 23:41–57, 1978.

[25] M. Hines and J. J. Blum. Bend propagation in flagella II. Incorporation of dynein cross-bridge kinetics into the equations of motion. *Biophysical Journal*, 25:421–442, 1979.

[26] K. Ishimoto and E. A. Gaffney. Squirmer dynamics near a boundary. *Physical Review E*, 88:062702, 2013.

[27] K. Ishimoto and E. A. Gaffney. A study of spermatozoan swimming stability near a surface. *Journal of Theoretical Biology*, 360:187–199, 2014.

[28] K. Ishimoto and E. A. Gaffney. Swimming efficiency of spherical squirmers: Beyond the Lighthill theory. *Physical Review E*, 90:012704, 2014.

[29] K. Ishimoto and E. A. Gaffney. Fluid flow and sperm guidance: a simulation study of hydrodynamic sperm rheotaxis. *Journal of The Royal Society – Interface*, 12:20150172, 2015.

[30] Y. Jia, Z. Meng, X. Liu, and J. Le. Biochemical composition and quality of turbot (*Scophthalmus maximus*) eggs throughout the reproductive season. *Fish Physiology and Biochemistry*, 40:1093–1104, 2014.

[31] R. Johnson. An improved slender-body theory for Stokes flow. *Journal of Fluid Mechanics*, 99:411–431, 1980.

[32] R. E. Johnson and C. J. Brokaw. Flagellar hydrodynamics: A comparison between resistive-force theory and slender-body theory. *Biophysical Journal*, 25:113–127, 1979.

[33] D. F. Katz and R. Yanagimachi. Movement characteristics of hamster spermatozoa within the oviduct. *Biology of Reproduction*, 22:759–764, 1980.

[34] J. Klein, A. Clapp, and R. B. Dickinson. Direct measurement of interaction forces between a single bacterium and a flat plate. *Journal of Colloid and Interface Science*, 261:379–385, 2003.

[35] J. Lighthill. Flagellar hydrodynamics - JV Neumann lecture. *SIAM Review*, 18:161–230, 1976.

[36] C. B. Lindemann and K. A. Leisch. Flagellar and ciliary beating: the proven and the possible. *J. Cell Sci.*, 123:519–528, 2010.

[37] R. Miller. Sperm chemotaxis in the hydromedusae. I. Species-specificity and sperm behavior. *Marine Biology*, 53:99–113, 1979.

[38] C. Pozrikidis. *A Practical Guide to Boundary Element Methods with the Software Library BEMLIB*. CRC, 2002.

[39] M. Psenicka, S. Alavi, M. Rodina, D. Gela, J. Nebesarova, and O. Linhart. Morphology and ultrastructure of Siberian sturgeon (*Acipenser baerii*) spermatozoa using scanning and transmission electron microscopy. *Biology of the Cell*, 99:103–115, 2007.

[40] I. H. Riedel-Kruse, A. Hilfinger, J. Howard, and F. Julicher. How molecular motors shape the flagellar beat. *HFSP Journal*, 1:192–208, 2007.

[41] R. Rikmenspoel. Movements and active moments of bull sperm flagella as a function of temperature and viscosity. *Journal of Experimental Biology*, 108:205–230, 1984.

[42] R. Rikmenspoel. Algebraic expressions for the waveforms of sea urchin sperm flagella. *J. Theoretical Biology*, 116:127–147, 1985.

[43] Rothschild. Non-random distribution of bull spermatozoa in a drop of sperm suspension. *Nature*, 198:1221–1222, 1965.

[44] J. Sharp and R. B. Dickinson. Direct evaluation of dlvo theory for predicting long-range forces between a yeast cell and a surface. *Langmuir*, 21:8198–8203, 2005.

[45] H. Shum, E. Gaffney, and D. Smith. Modelling bacteria behaviour close to a no-slip plane boundary: the influence of bacterial geometry. *Proceedings of the Royal Society of London A*, 466:1725–1748, 2010.

[46] D. J. Smith, E. A. Gaffney, J. R. Blake, and J. C. Kirkman-Brown. Human sperm accumulation near surfaces: a simulation study. *Journal of Fluid Mechanics*, 621:289–320, 2009.

[47] D. J. Smith, E. A. Gaffney, H. Gadêlha, N. Kapur, and J. Kirkman-Brown. Bend propagation in the flagella of migrating human sperm, and its modulation by viscosity. *Cell Motility and the Cytoskeleton*, 66:220–236, 2009.

[48] D. J. Smith, E. A. Gaffney, H. Shum, H. Gadhêla, and J. C. Kirkman-Brown. Comment on the article by j. elgeti, u. b. kaupp, and g. gompper: Hydrodynamics of sperm cells near surfaces. *Biophys. J.*, 100:2318–2320, 2011.

[49] S. E. Spagnolie and L. Lauga. Hydrodynamics of self-propulsion near a boundary: predictions and accuracy of far-field approximations. *Journal of Fluid Mechanics*, 700:105–147, 2012.

[50] M. Suquet, R. Billard, J. Cosson, G. Dorange, L. Chauvaud, C. Mugnier, and C. Fauvel. Sperm features in turbot (*Scophthalmus maximus*): a comparison with other freshwater and marine fish species. *Aquatic Living Resources*, 7:283–294, 1994.

[51] M. Suquet, G. Dorange, M. Omnes, Y. Normant, A. Le Roux, and C. Fauvel. Composition of seminal fluid and ultrastructure of the spermatozoon of turbot (*Scophthalmus maximus*). *Journal of Fish Biology*, 42:509–516, 1993.

[52] M. Suquet, C. Dreanno, C. Fauvel, J. Cosson, and R. Billard. Cryopreservation of sperm in marine fish. *Aquaculture Research*, 31:231–243, 2000.

[53] D. M. Woolley. Motility of spermatozoa at surfaces. *Reproduction*, 126:259–270, 2003.

[54] R. Yanagimachi, G. Cherr, T. Matsubara, T. Andoh, T. Harumi, C. Vines, M. Pillai, F. Griffin, H. Matsubara, T. Weatherby, and K. Kaneshiro. Sperm attractant in the micropyle region of fish and insect eggs. *Biology of Reproduction*, 88:1–11, 2013.

[55] R. Yanagimachi, G. Cherr, C. Muralidharan, and J. Baldwin. Factors controlling sperm entry into the micropyles of salmonid and herring eggs. *Development Growth and Differentiation*, 34:447–461, 1992.